Modified Sliding Mode Control and its Application to Electrostatically Controlled Dual-Axis Micromirrors

Harshad S. Sane, Navid Yazdi, and Carlos H. Mastrangelo

***Abstract*— In this paper, we demonstrate the application of a modified sliding mode control (SMC) scheme with time-constant switching for MEMS micromirror control. This scheme yields substantial performance improvement over previous work, without increasing in implementation complexity. The modification implements a discrete first-order sliding function with a switching time constant and provides the same level of robustness with an added benefit of reduced steady-state error. A two-axis gimbaled MEMS micromirror array designed at Corning-Intellisense is used for experimental demonstration.**

I. INTRODUCTION

THE fast-growing optical-fiber communication network requires low-cost reliable optical devices to implement the fiber-to-the-home concept [1,2] and micromirrors are often used for implementing optical cross-connects (OXC) [6,10]. In order to obtain a few tenth's of dB optical power stability an angular pointing accuracy of milli-degrees is typically required [13]. A micromirror deflection range of at least ±15 degrees is preferred [5,6] to allow increase of the number of ports without increasing the optical path length and optical losses. The angular deflection is generally limited by the instability due to electrostatic actuation. The controller is additionally required to be compact, tolerant of micromirror characteristic variations due to lithographic variations and manufacturing tolerances, and fast with a switching time of ~10 milli-seconds or less. Here, switching time is defined as the time after which the steady state error is within 100 μrad. Therefore, the choice of control algorithm becomes critical in ensuring the robustness and stability over all operational conditions.

Linear closed-loop control methods [11] and algorithms based on non-linearity inversion [8] depend on knowing nonlinear characteristics of the actuator. Hence, they could require extensive gain scheduling and do not necessarily guarantee stability in presence of parametric uncertainties. In [12] we proposed the application of sliding mode control (SMC) algorithm. The main arguments in favor of SMC [7, 14-18] are robustness, computation speed, easy controller implementation, and disturbance rejection. A well-known characteristic of SMC is that it requires a high chattering control activity on the actuating drive. While chattering is a problem for conventional actuators with bandwidth limitation, it is not a concern for electrostatic MEMS actuators with high-speed digital drive circuits. In fact this is the tradeoff that is desired: rapid digital switching replacing analog control.

Our eventual goal is to implement the control algorithm on application specific integrated circuits (ASIC) with embedded capacitive sense and control circuits. This is aimed to promote modular functionality, facilitate scalability [5,6,13] and greatly reduce loop delays. The area constraints posed by this goal restricts the complexity of control scheme to be implemented. Sliding mode control ideally suits this need as it can be implemented simply by means of switches and comparators.

Using numerical simulations and experimental tests [12], we showed that SMC yields stable operation over the desired range of angular deflection and stability and switching time performance is robust to the expected parametric variations. However, it was observed that discrete-time implementation of SMC led to inconsistent chattering performance and the steady state errors (SSE) that varied depending on the operating point and torque nonlinearities. In this paper, we propose a modification to the SMC algorithm that attempts to reduce these errors. Numerical simulation results show that the modified scheme yields ~40% attenuation of output chatter and ~70-90% reduction of steady state error. These observations are validated using experimental implementation.

In Section II, we briefly describe the micromirror device manufactured at Corning-IntelliSense. In Section III, we introduce the SMC algorithm and summarize its robustness properties as reported in [12]. In Section IIIB, we discuss the errors resulting from discrete-time implementation and present the modified SMC algorithm (Section IIIC) that attempts to reduce these errors. In Section IV we present numerical and experimental results for the micromirror system and compare the performance using nominal SMC and the proposed modified SMC scheme.

II. ELECTROSTATICALLY ACTUATED MICRO-MIRROR

The micromirror (Fig. 1) has a dual-axis gimbaled structure and is fabricated using a combined bulk and surface micromachining process [9]. The mirror is actuated using a pair of electrodes per axis situated underneath the mirror. The outer frame is 1500μm wide and the inner mirror has a radius of about 440μm. The inner mirror and

Manuscript received Mar 1, 2004. This work was supported in part by Corning, Inc. and Advanced Technology Program (ATP Award No. 70NANB2H3043) of National Institute of Standards and Technology.

Authors are IEEE members with Corning-IntelliSense, Inc., Wilmington, MA01887. (978) 9888000; e-mail: harshad@engin.umich.edu

outer frame have a deflection range of ±15° and experimental determination of deflection-vs.-voltage curve indicated an electro-statically stable range of ~8° at <260V for each axis. This angle is called the *pull-in angle* of the device.

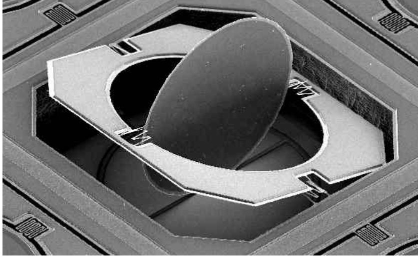

Fig. 1: Photograph of 2-axis gimbaled micromirror array.

A. Dynamical Model

Let ρ , η be the angular positions and $T_m(\rho,\eta,V_m,V_f)$, $T_f(\rho,\eta,V_m,V_f)$ be the electrostatic torques on the inner and outer axis, respectively. Here V_m and V_f are the control voltages applied to the electrodes. The dynamics of the electrostatically actuated MEMS can be written as

$$\begin{aligned} \ddot{\rho} + 2\gamma_m \omega_m \dot{\rho} + \omega_m{}^2 \rho &= \frac{1}{I_m} T_m(\rho,\eta,V_m,V_f) \\ \ddot{\eta} + 2\gamma_f \omega_f \dot{\eta} + \omega_f{}^2 \eta &= \frac{1}{I_f} T_f(\rho,\eta,V_m,V_f) \end{aligned}, \tag{1}$$

where ω_m , ω_f are resonance frequencies, γ_m , γ_f are the damping coefficients, I_m and I_f are the moments of inertia for the inner and outer axis, respectively. Since the electrostatic force is inversely proportional to square of the local gap, the angular dynamics (1) are coupled due to the nonlinear torques T_m and T_f . For more details on the properties of the two-axis micromirror system, see [12].

B. Model Parameter and Uncertainties

The dynamical properties of the MEMS, such as the stiffness, moments of inertia, and damping are estimated using *IntelliSuite*™ FEM/BEM CAD software. These values are verified experimentally. The resonance frequencies for the inner and outer angular dynamics were found to be in the range of 80-130Hz with a quality factor of 5 and 3, respectively. The resonance frequency is expected to vary about ±25% and the Q-factor has an expected variation of about ±50% across the wafer due to uncertainties in fabrication process. Electrostatic torque characteristics are obtained using FEA and curve fitted to yield a multivariate function of V_m, V_f , ρ and η . Figure 2 shows an instance of this function for the inner axis torque for control voltages $V = \pm 200$V.

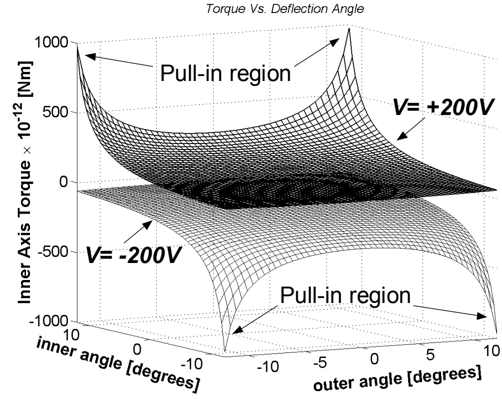

Fig. 2: Electrostatic torque on inner axis as a function of deflection angles with ±200V drive.

III. Sliding-Mode Control

In [12] we showed the applicability of sliding mode control (SMC) to the micromirror system and demonstrated successful stabilization and tracking in simulation and experimentation. We consider a first-order SMC with the sliding-manifold *s(e)* given by

$$s = e + \tau \frac{de}{dt}, \tag{2}$$

where *e* is the error between the deflection angle and the set point, and the τ is the time-constant of convergence. The control input *u* given by

$$u(s) = \begin{cases} +V, \text{if } s(e) \le 0 \\ -V, \text{if } s(e) > 0 \end{cases}. \tag{3}$$

The sliding mode controller switches between two unstable open-loop phase portraits (see [12] for more details) to yield a first-order closed-loop response that decays exponentially with time constant τ.

A. Robustness

For discrete-time implementation of sliding mode control with sample time Δt , the sliding mode function in equation (2) can be re-written as

$$\begin{aligned} s_\rho(k) &= e_\rho(k) + D_\rho(e_\rho(k) - e_\rho(k-1)) \\ s_\eta(k) &= e_\eta(k) + D_\eta(e_\eta(k) - e_\eta(k-1)) \end{aligned}, \tag{4}$$

where $e_\rho(k)$, $e_\eta(k)$ are the angle errors, and $D_\rho = \tau_\rho / \Delta t$, $D_\eta = \tau_\eta / \Delta t$ are referred as differential gains (D-gain) for the inner and outer angle sliding mode controllers, respectively. The main virtue of SMC, namely robustness, was demonstrated [12] using simulations by varying the dynamical properties such as resonance frequencies and damping within the expected variations in fabrication. After reaching the sliding manifold, the trajectories of the closed-loop system are governed by (2) and are independent of system parameters such as stiffness, damping and moment of inertia. It was shown that the closed-loop system showed

less than ±20% variation in switching (settling) time performance. However, it was observed that discrete-time implementation led to inconsistent chattering performance and the steady state errors that varied depending on the operating point and torque nonlinearities. The next section described these errors in more detail.

B. Sources of Errors in Discrete-time Implementation

In sampled-data systems the control can switch only as fast as the sampling rate $f_s = 1/\Delta t$. In previous sections, (2) was implemented in the discrete-time form (4) where $D = \tau/\Delta t$ is the differential gain (D-gain). Using (1), the error dynamics for both axes can be written in the form

$$\ddot{e} + 2\zeta\omega\dot{e} + \omega^2 e = \frac{1}{I}(T - K\theta_{set}), \quad (5)$$

where e is the angle error, T is the torque, $K = I\omega^2$ is the spring constant, and θ_{set} is the set-point angle. Between samples, the control input is fixed at one of the two voltage values in (3) and the trajectory "coasts" away from the sliding mode leading to chattering. The *residual torque* T_{res}, is defined as the excess electrostatic torque over restoring spring torque and is given by $(T(V,\theta_{set}) - K\theta_{set})$. Let $T_{res}^{+} = T(V,\theta_{set}) - K\theta_{set}$ and $T_{res}^{-} = T(-V,\theta_{set}) - K\theta_{set}$ be the residual torques for positive and negative control inputs, respectively. Using (5), we can see that close to the origin (neglecting effect of damping ζ during the sample time) the trajectories appear as concentric arcs on the phase plane e vs. $\dot{e}$ with centers at (T_{res}^{+}/K,0) and (T_{res}^{-}/K,0) for positive and negative control inputs, respectively.

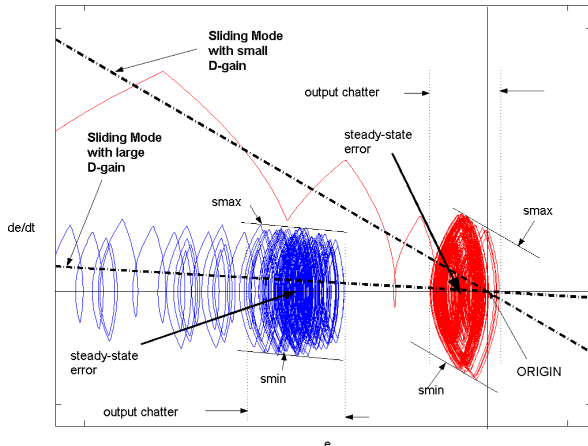

Fig. 3: Discrete-time sliding mode behavior as a function of time constant τ.

In Figure 3 the phase plots shows the sliding mode trajectory for low and high differential gain $D = \tau/\Delta t$. This simulation corresponds to an outer axis setpoint of 12° and a sampling rate of 75kHz. At the midpoint of the centers ($(T_{res}^{+} + T_{res}^{-})/2K$,0), the arcs have equal radii and equal arc lengths per unit time.

Using (5), we note that near the setpoint, the derivative of the sliding mode function is given by

$$\dot{s} \approx (1 - 2\tau\zeta\omega)\dot{e} + \frac{\tau}{I}T_{res}. \quad (6)$$

Due to the nonlinearity in the torque, control inputs of equal magnitudes (±*V*) can lead to unequal values of residual torques, T_{res}^{+} and T_{res}^{-} at some deflections. In the micromirror system, plots of inner and outer axis torques (Fig. 4) show that although the residual torques are closely matched at 2°, they are significantly different in magnitude at 10°. In case of mismatch in residual torques the sliding mode trajectory travels further for one value of control input in a given sample interval, leading to steady state error. From (6) we note that since $\dot{s}$ is proportional to $\tau T_{res} = DT_{res}\Delta t$, a higher D leads to higher output chatter. Let $\dot{s} = v^{+}>0$ and $\dot{s} = v^{-}<0$ be the sliding-mode derivative for $T_{res} = T_{res}^{+}$ and $T_{res} = T_{res}^{-}$, respectively. It can be easily shown that [17] the average value of $s(e,\dot{e})$ at steady state is given by

$$s_{av} \approx \frac{1}{2}(v^{+} + v^{-})\Delta t. \quad (7)$$

Qualitatively speaking, using (7) and phase plane trajectories in Figure 3, we can say that the steady state *on the sliding manifold* is reached when the concentric arcs for positive and negative residual torques match each other; that is intersect each other with same arc-lengths per unit time. For a large τ the sliding mode is flatter and the matching of the concentric arcs happens away from the origin and closer to the mid-point of the centers of the arcs ($(T_{res}^{+} + T_{res}^{-})/2K$, 0). An increased mismatch in the residual torques results in a larger steady state error, as the midpoint is further away from the origin. For a small τ, the sliding mode is steeper and the matching of arcs *on the sliding mode* (similar arc-length per unit time) occurs closer to the origin, resulting in a lower steady state error.

A faster controller (smaller Δt) ensures lower output chatter but requires a high differential gain D to maintain the same τ. In mixed-signal ASIC implementation it is not desirable to have signal-amplifiers with large gains. Lastly, due to lithography and process variations, it is extremely difficult to remove the effects of mismatch in residual torques by design and maintain closed-loop robustness.

C. D-gain Switching Scheme

The errors discussed in the previous section can be minimized by using higher-order sliding-mode function [3, 14], or boundary layer based sliding mode control [15,18]. Other alternatives [17,18], that include introducing integrators and observer based sliding mode control, do not attempt to solve the problems due to discrete-time

implementation. Introducing integrators reduces the robustness of the closed-loop system. These methods require additional computational effort making it difficult to implement under circuit area constraints. More importantly, since optical switching applications demand high precision pointing (with specifications within 100 μrad), it warrants a high-speed implementation.

From Section IIIB, we know that the errors at steady state increase as τ increase. We propose a simpler solution that attempts to minimize these errors by switching the differential gain $D = \tau / \Delta t$, within a switching gap about the desired set point. We refer to this scheme as the "D-gain switching scheme". The switching is defined by gap parameter $d > 0$, and attenuation factor $\gamma < 1$, so that

$$D = \begin{cases} D_0, \text{ for } |e| > d \text{ (outside switching gap)} \\ \gamma D_0, \ |e| < d \text{ (inside switching gap)}, \gamma < 1 \end{cases}. \quad (8)$$

where D_0 is the nominal differential gain. The parameters d and $\gamma < 1$ are chosen in order to avoid overshoot and ensure minimum attraction for stable operation. In short, the proposed modification to the SMC avoids overshoot by weighing the derivative higher during slewing and reduces steady state errors by lowering the differential gain while settling. This scheme can be easily implemented in integrated circuits as it only requires switches and comparators.

IV. Application of Modified-SMC to the Micromirror System

A. Numerical Simulations

The simulation setup is designed to model the experimental setup as accurately as possible. The setup consists of an incident beam reflecting off the MEMS onto a position sensing detector (PSD) array. The PSD array has a voltage output pair linearly depending on the position *(x, y)* of the incident beam with the center of the PSD corresponding to (0*V*, 0*V*). The PSD output on each axis can be modeled as a trigonometric function of MEMS angular deflections angles. In the experimental setup, this function is given by $V = 31.2\tan(2\theta pi/180)$ where θ is the deflection angle. Measurement delays of 5μs are assumed on PSD outputs. For sliding mode control, the set points ρ_{set} and η_{set} are specified in terms of their equivalent PSD voltages. Simulations are conducted with a sampling rate of 75kHz.

The parameters for the modified switching scheme are chosen to have a switching gap of $d = 0.1V$ (~0.08°) and D-gain factor γ =0.1 for inner axis and outer axis control. Figure 4 show the outer-axis angle plot for a numerical simulation where the set-points were chosen to be (12°,12°). The solid line depicts the standard SMC scheme (non-switching) and dashed line corresponds to the D-gain switching scheme. The switching band is indicated by two horizontal dotted lines. Figure 5 shows the respective phase plane trajectories for the outer axis that clearly shows the switching to the "steeper" sliding mode. The corresponding figure for the inner axis is omitted due to space constraints.

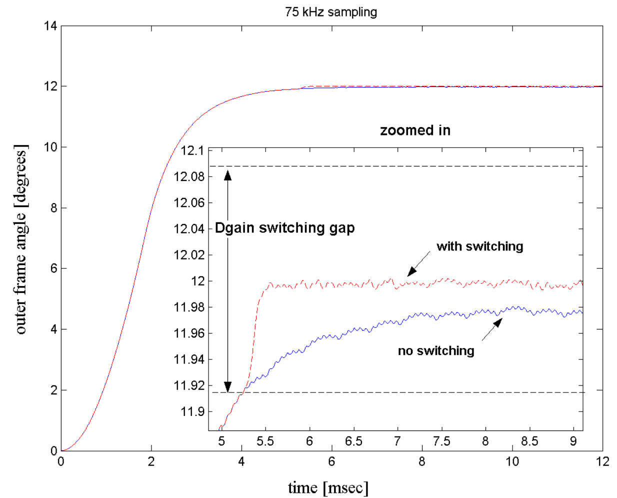

Fig. 4: Outer Axis: Comparison of Dgain switching scheme with conventional SMC.

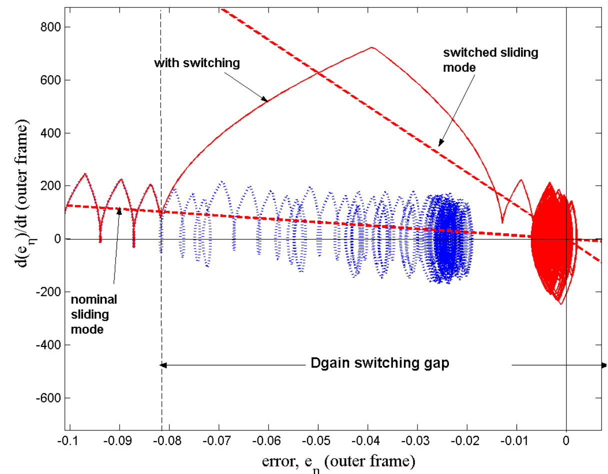

Fig. 5: Comparison of Dgain switching scheme with the nominal discrete SMC scheme (phase portraits – zoomed in).

	Output chatter		Steady state error	
	No switching	With switching	No switching	With switching
Mirror	4.67 mdeg	3.7 mdeg	-20.5 mdeg	-3.5 mdeg
Frame	6.09 mdeg	1.95 mdeg	-26.1 mdeg	-2.86 mdeg

Table 1: Improvement with D-gain Switching

Table 1 gives a quantitative summary of the improvements shown in these figures. Note that the scheme yields a substantial (80-90%) reduction in steady state error. It is also observed that the output chatter is reduced by 30-40%. Furthermore, the trajectory satisfies the 100 μrad

pointing criteria in less time yielding reduced switching time.

B. Experimental Results

1) Experimental Setup

The experimental setup includes the mirror array, a laser light source, a PC-based DSP board, and a *Hamamatsu* C4674 position sensing diode (PSD) based angular measurement system. Figure 6 shows the picture of the experimental design verification test setup. The MEMS array is mounted vertically and a desired mirror is illuminated with a red laser (with the help of a high magnification video camera). The reflected light is calibrated to the center of the PSD for zero deflection.

A PC is used to implement the SMC for a single device of the micromirror array. The PSD provides X (outer axis) and Y (inner axis) analog voltages proportional to the beam displacement from the PSD center. The PSD output has a gain of 1V/mm and an equivalent angle noise of 5milli-degrees-rms.

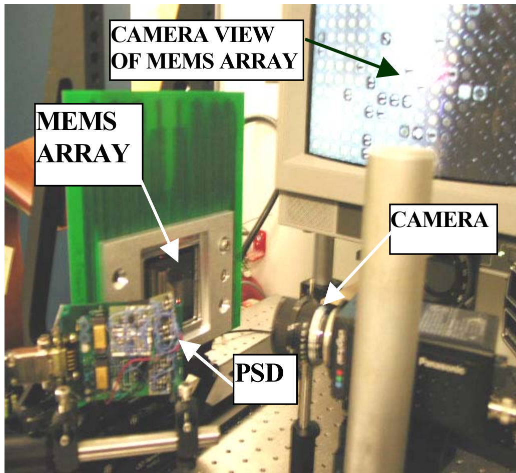

Fig. 6: Picture of the design verification test setup

A visual C based GUI in conjunction with an assembly code is used for running the modified algorithm at 150kHz. The effective SMC loop sampling rate (f_s) is 75kHz as the measurements are multiplexed between the x and y axes. The phase lag from the position sampling to applying the feedback is ~5µsec. Unlike the simulation environment, the distance of mirror array from the PSD allows only a restricted deflection range in both axes. The output range of PSD is between -5.0 V to 5.0V (±4.58°) for each axis. The setpoint is specified in terms PSD voltages.

2) Results

Using experimentally obtained deflection-vs-voltage data, it was determined the micromirror has pull-in angle ~8° at <260V drive voltage for each axis. In Figure 7, we show a representative result (oscilloscope capture) for a switch beyond the pull-in limit. The measured switching time is < 3 ms. Several micro mirror devices having a fairly wide range of angle versus voltage characteristics (200-310V), quality factors (2.0-6.0) and resonant frequencies (78-150 Hz) (induced by variations in device thickness, spring constant values and misalignment errors) have been tested with the SMC scheme with similar performance.

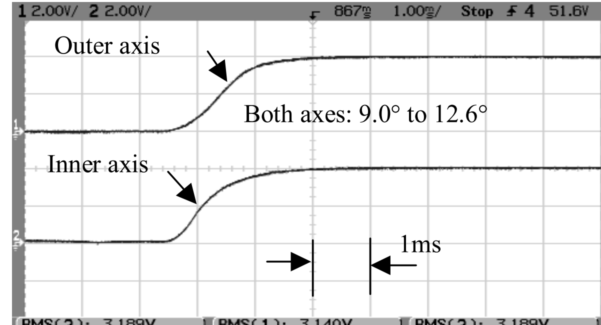

Fig. 7: Measured step response of the 2-axis micromirror beyond the pull-in limit.

For the modified sliding mode control scheme, we choose a switching gap with d=*0*.2V (~0.176°) and the attenuation factor γ is varied between 0.1 and 1. Figure 8 shows a oscilloscope capture showing the switching response from 0°-3.58° on each axis. The measured errors (shown below the figure) indicate about 80-90% reduction in steady state error (SSE) and 40-50% reduction in output chatter.

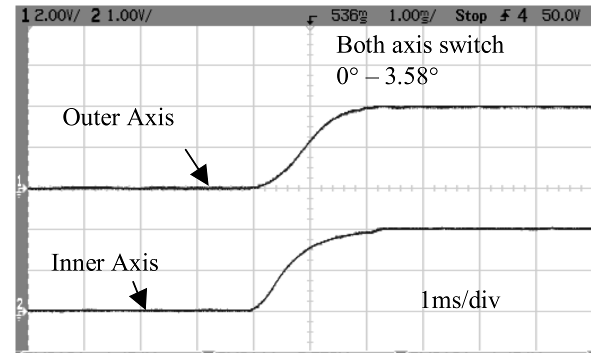

Dgain switching with d=*0*.2V, $\gamma = 0.1$. SSE (X,Y):-0.002°, 0.007°, Output chatter (X,Y): 7 mdeg, 12 mdeg
Compare to **Nominal discrete-time SMC:** SSE (X,Y): -0.031°, -0.063°, Output chatter (X,Y): 13.0 mdeg, 19 mdeg

Fig. 8: Experimental switching result with the modified SMC scheme.

Figure 8 shows a "latching" of the trajectory (similar to Figure 4) towards the switched sliding mode as it enters the switching band. In the test setup, several mirrors were tested using the modified sliding mode control scheme and Figure 9 shows average improvement over all tested mirrors. It can be seen that the scheme yields consistent improvement with decrease in γ or the differential gain. For $\gamma = 0.1$ we

obtain about 44-56% output chatter reduction and about 70-91% steady state offset. Similar improvements are obtained while switching at high angles.

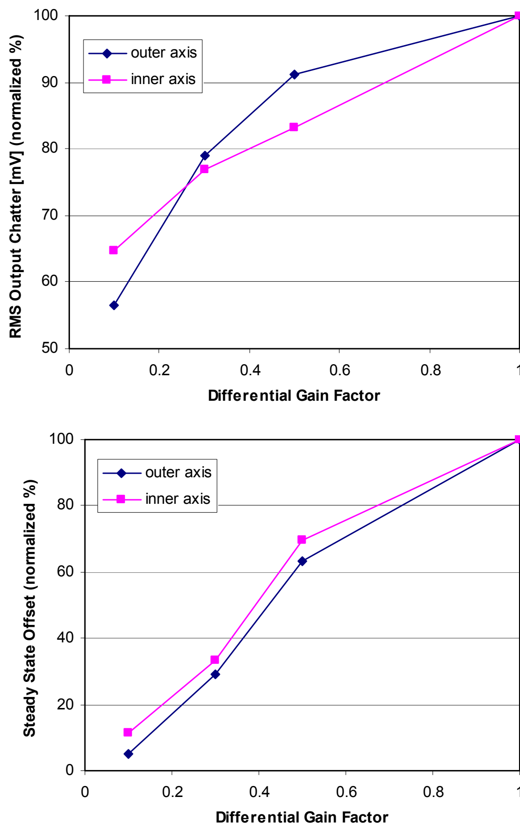

Fig. 9: Effect of differential gain on steady state errors. Experimental results for switching from 0° to 4°. Plots show performance normalized (%) to performance with unmodified sliding mode control.

C. Conclusions and Future Work

In this paper, we present the application of a modified sliding mode control scheme with switching time-constant to MEMS micromirror developed at Corning-IntelliSense Inc. We discuss the sources of errors involved due to discrete-time implementation of the controller and conclude that these errors are attributed to the sampling time and the time constant of the SMC. Numerical simulation results show that this scheme yields about 70-90% reduction of steady state error. The scheme is validated in experiments MEMS micromirror test system and similar improvements are observed. Our future efforts would be focused on investigating schemes to maintain and enhance the robustness and performance of the SMC. Alternate adaptive versions of SMC are being investigated which involve adaptive pulse-width/height modulation techniques [7] in order to reduce the effect of mismatch in residual torque. These modifications are researched by keeping in perspective our eventual goal of implementing these controllers on ASICs with on-chip sense and control logics circuitry.

REFERENCES

[1] D. J. Bishop, C. R. Giles, and S. R. Das, "The Rise of Optical Switching", Scientific American, pp. 88-94, Jan 2001.

[2] D. Bishop, "The Lucent Lambdarouter: MEMS technology of the future here today", IEEE Communications Mag., vol.40(8), pp. 75-79.

[3] S. V. Drakunov and V. I. Utkin, "Sliding mode in dynamic systems," International Journal of Control, vol 55, pp. 1029-1037, 1990.

[4] A. Fillipov, Differential Equations with Discontinuous Right-Hand-Sides, Kluwer Academic Press, 1988.

[5] P. M. Hagelin et. al., "Scalable Fiber Optic Switch Using Micromachined Mirrors," Proc. 10th Int. Conf. Solid –State Sensors and Actuators (transducers"99), Sendai, Japan, June 7-10, 1999, 2P6-2.

[6] S. H. Hinton, An Introduction to Photonic Switching Fabrics, Plenum, 1993.

[7] U. Itkis, Control Systems of Variable Structure, John Wiley & Sons, New York, NY, 1976.

[8] T. Juneau, et al, "Dual-Axis Optical Mirror Positioning using a Nonlinear Closed-Loop Controller," Transducers, Int. Conf. Solid-State Sensors, Actuators and Microsystems, pp. 560 – 563, Boston, MA, June 2003.

[9] T. Kudrle, G. Shedd*, C. C. Wang, J. C. Hsiao, M. G. Bancu, G. A. Kirkos, N. Yazdi, M. Waelti, H. Sane, and C. H. Mastrangelo, "Pull-in Suppression and Torque Magnification in Parallel Plate Electrostatic Actuators with Side Electrodes," Transducers, Int. Conf. Solid-State Sensors, Actuators and Microsystems, pp. 360 – 363, Boston, MA, June 2003.

[10] L. Y. Lin, E. L. Goldstein, and R. W. Tkach, "Free-space Micromachined Optical Switches for Optical Networking," IEEE J. Select. Topics Quantum Electron: Special Issue on Microoptoelectromechanical Systems (MOEMS), vol. 5, 1999, pp. 4-9.

[11] M. S. Lu, G. Fedder, "Closed-Loop Control of a Parallel-Plate Microactuator Beyond the Pull-In Limit," Tech. Dig. Solid-State Sensor, Actuator and Microsystem Workshop, Hilton-Head, SC, 2002, pp. 255-258.

[12] H. Sane, N. Yazdi, and C. Mastrangelo, "Application of Sliding Mode Control to Electrostatically Actuated Two-Axis Gimbaled Micromirrors," Proceedings American Control Conference, pp. 3726–3721, Denver, CO, June 2003.

[13] R. A. Syms, "Scalable Laws for MEMS Mirror-Rotation Optical Cross-Connect Switches," J. Lightwave Tech., vol. 20, no. 7, July 2002.

[14] W. C. Su, S. V. Drakunov, U. Ozguner, and K. D. Young, "Sliding mode with chattering reduction in sampled data systems," in Proc. 32nd IEEE Conf. Decision Contr., San Antonio, TX, Dec. 1993, pp. 2452–2457.

[15] W. Su, S. V. Drakunov, and U. Ozguner, "An O(T2) Boundary Layer in Sliding Mode for Sampled-Data Systems," IEEE Trans. Automat. Contr., vol. AC-45, no.3, pp. 482-485, 2000.

[16] V. I. Utkin, "Sliding mode control is discrete-time and difference systems," in A. Zinober, (Ed.), Variable Structure and Lyapunov Control, Springer-Verlag, London, 1993.

[17] V. Utkin, J. Guldner, and J. Shi, Sliding Mode Control in Electromechanical Systems, Taylor & Francis, Philadelphia, PA, 1999.

[18] D.Q Zhang and S.K. Panda, "Chattering-free and fast-response sliding mode controller," IEE Proceedings Control Theory and Applications, Volume: 146 Issue: 2, pp. 171-177, March 1999.